In situ determination of indium/gallium composition in InxGa1-x nanodroplets on GaAs(111)A based on the complementarity between XPS and REELS

Romain Jouanneaud, G. Monier, Luc Bideux, Nicolas Pauly, Christine Robert-Goumet

In situ determination of indium/gallium composition in In_xGa_{1-x} nanodroplets on GaAs(111)A based on the complementarity between XPS and REELS

Romain JOUANNEAUD[1], Guillaume MONIER[1,*], Luc BIDEUX[1], Nicolas PAULY[2], Christine ROBERT-GOUMET[1]

[1] *Université Clermont Auvergne, Clermont Auvergne INP, CNRS, Institut Pascal, F-63000 Clermont-Ferrand, France*
[2] *Université Libre de Bruxelles, Service de Métrologie Nucléaire (CP 165/84), 50 av. F. D. Roosevelt, B-1050 Brussels, Belgium*

** Corresponding author. E-mail address: guillaume.monier@uca.fr (G. Monier).*

Abstract

This work provides a new tool based on the complementarity between X-ray Photoelectron Spectroscopy (XPS) and Reflection Electron Energy Loss Spectroscopy (REELS). More precisely, this study is focused on the *in situ* precise determination of indium and gallium composition of self-assembled In_xGa_{1-x} nanodroplets on GaAs(111)A substrate during the first stage of III-V quantum dots growth by droplet epitaxy. An XPS intensity model based on In4d and Ga3d core levels enables the estimation of the gallium/indium ratio within the droplets under the assumption of a homogeneous droplet. On the other hand, we develop a brand new decomposition methodology of loss probabilities curves obtained from REELS spectra for droplets deposited on a substrate. The energy of In_xGa_{1-x} bulk plasmon experimentally obtained and semi-empirically modelled allows to calculate from REELS the indium-gallium composition in the droplet. Comparison between these values obtained by both XPS and REELS provides information about In/Ga mixing to grow binary In_xGa_{1-x} nanodroplets. Their good agreement shows promising results for the growth of $In_xGa_{1-x}N$ quantum dots by droplet epitaxy for a very large range of composition.

Keywords : *XPS, REELS, GaAs substrate, InGa self-assembled droplets, indium content, droplet epitaxy*

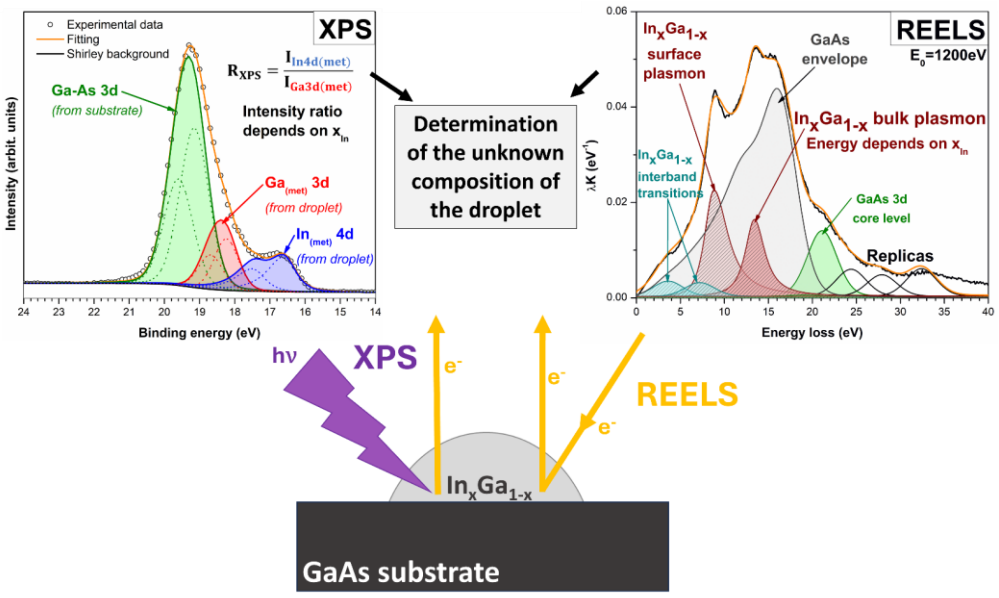

1. Introduction

Ternary compounds such as indium gallium nitride ($In_xGa_{1-x}N$) provide well-established wavelength tunability by controlling indium content that is promising for a large range of optoelectronics applications. More recently, InGaN nanostructures, and more precisely InGaN quantum dots (QDs), have attracted attention for their unique properties involving their potential use for optoelectronic devices such as LED, laser diodes and single photon emitters [1–5].

QDs of semiconducting materials were firstly grown by Stranski-Krastanov (SK) mode. But the requirement of a large mismatch between the substrate and the epitaxial layer to initiate QD growth is one of the drawbacks. Such induced stress could lead to structural defects and dislocations that reduce their use for optoelectronic applications. Recently, droplet epitaxy (DE) has emerged as a promising method to grow GaAs [6,7], GaN [8–11] and InN [12–14] QDs on semiconductor substrates. First stage of DE is the deposition of III-metallic (In, Ga) self-assembled droplets on the substrate followed by a second stage consisting in the supply of the V element (N, As). DE allows a better control of the QDs density and both composition and size homogeneity than SK, and can be applied to a large range of substrates, including homoepitaxial growth. Recent study shows high-density, high-indium composition and polycrystalline InGaN QDs grown by DE on nitrided Si(111) substrate [15] confirming the potential of DE for ternary compounds QDs growth.

One of the issue relies on the precise determination of indium content in $In_xGa_{1-x}N$ nanostructures. It is usually achieved by the measurement of the lattice constant in X-Ray Diffraction [16–18], Transmission Electron Microscopy (TEM) [19] and Rutherford Backscattering Spectroscopy [20] or by the bandgap measurement in photoluminescence [4,21,22]. Indium content is then determined using the empirical Vegard's law [23]. Indium content can also be determined by Energy Dispersive Xray Spectroscopy [24], as shown in [25] for nanowires. Some studies [15,26] try to estimate the chemical composition of InGaN QDs on Si substrate, but the quantification methodology is not presented.

With the exception of XPS, most of the quoted methods require to be done *ex-situ* and are based on the crystallinity of the studied materials. However, during first stage of droplet epitaxy, InGa droplets are amorphous. To the best of our knowledge, they are few studies allowing the characterization of indium content in In_xGa_{1-x} alloy ; one relies on the chemical destructive process based on anodic voltammetry [27]. A relevant tool to control the composition and the organisation of the deposited atoms is then required to perform DE of InGaN quantum dots. We provide in this work the complementary use of X-ray Photoelectron Spectroscopy (XPS) and Reflection Electron Energy Loss Spectroscopy (REELS) for the *in-situ* determination of indium/gallium content in self-assembled In_xGa_{1-x} droplets on GaAs(111)A substrate.

2. Materials and methods

2.1. Experimental set-up

Our ultra-high vacuum ($P \approx 10^{-10}$ mbar) assembly is composed by introduction, preparation and SPECS Provent-XPS analysis chambers. It allows both the *in-situ* deposition of III-metallic droplets (In, Ga, In_xGa_{1-x}) and the analysis by a combination of electronic spectroscopies (REELS, XPS) using a SPECS PHOIBOS-150 hemispherical analyser with 2D-CMOS detector.

REELS investigates the inelastic interactions between an E_0 monoenergetic electron beam and the material by collecting the backscattered electrons. REELS spectra are *in-situ* acquired using an SPECS-PU-EQ-22 electron gun with primary energy ranging between 400 and 2000 eV located at an 30° incident angle to the normal of the sample. Analyser is running with a high magnification lens mode, a fixed pass energy E_{pass}=3 eV and an 0.1 eV energy step. Energy resolution is estimated to be around 0.5 eV using the full width at half maximum (FWHM) of the elastic peak and varies only slightly with primary energy.

XPS is performed with a monochromatic Al-Kα source (1486.6eV) running at 400 W, located at the 54.7° magic angle to the axis of the analyser. High magnification analyser lens mode is used, with an energy step of 0.1 eV and a constant pass energy of 20 eV. Energy resolution is estimated around 0.6 eV according to the width of Fermi level of polycrystalline silver foil previously cleaned by Ar^+ sputtering. REELS and XPS spectra are acquired with a 90° take-off angle corresponding to the normal direction compared to the surface sample.

NanoGrafi (Si-doped) and Wafer Technology (Zn-doped) GaAs(111)A 2'' commercial wafers are chemically cleaned by HCl/IPA before their quick introduction in the UHV assembly. Then, samples are annealed under vacuum at 530°C as described in reference [28]. XPS spectra show neither O1s nor C1s peak. For pure gallium and indium REELS references, the procedure based on the reference [29] is the same for both materials. Pure (99.999%) gallium (indium) sphere is crushed on stainless steel sample holder and is then *in situ* sputtered by an Ar^+ ion beam (E=1.5keV, I_{sample}≈2μA/cm²) for one hour to remove native oxides and surface contaminations. XPS shows pure material spectra, with a very low O1s peak intensity for both In and Ga.

Gallium and indium droplets are deposited on GaAs(111)A substrate using evaporation Knudsen-type cells where fluxes are calibrated with a quartz balance. The substrate temperature is monitored by a calibrated radiative system. Total amount of 3 monolayers (ML) of gallium and indium is simultaneously deposited with a total flux F_{tot}=0.10 ML/s. Relative fluxes of indium and gallium can be monitored to vary indium content, the relative flux of indium can be introduced as $R_f=F_{In}/F_{tot}$. Three series of samples with R_f varying from 0 (Ga droplets) to 1 (In droplets) corresponding to three different substrate temperatures: 180°C, 240°C and 350°C have been realized. Figure 1 shows a Scanning Electron Microscope (SEM) image for an R_f=0.8 and $T_{substrate}$=180°C deposition. The sample is 52° tilted to give an overview of the droplet morphology. The left side of the histogram, of the size distribution obtained from SEM image processing, is truncated because of the finite SEM resolution limit.

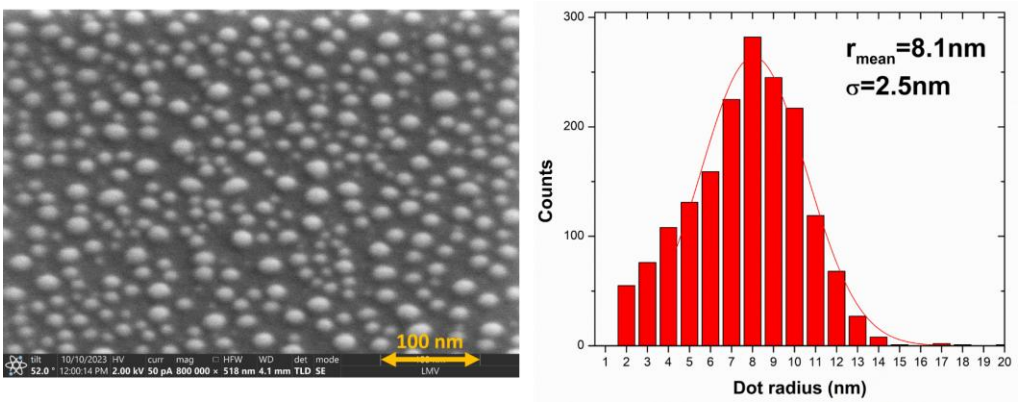

Fig. 1. 52° tilted view SEM image of an R_f=0.8 InGa simultaneous deposition on GaAs(111)A substrate ($T_{substrate}$=180°C)

2.2. XPS determination of gallium-indium content in the droplet

To determine the gallium-indium content in the droplet, XPS measurements have been performed. For this purpose, the intensity ratio R_{XPS} between the In4d and the Ga-metallic component of the Ga3d core levels intensities is calculated. Using the generic formula for XPS intensity [30] and under the assumption of an homogeneous droplet, this intensity ratio can be written as :

$$R_{XPS} = \frac{I_{In4d(met)}}{I_{Ga3d(met)}} \approx \frac{x_{XPS}}{(1 - x_{XPS})} \times \frac{\sigma_{In4d}}{\sigma_{Ga3d}} \#(1)$$

Where I is the intensity of the XPS peak, x_{XPS} the indium content in the droplet (1-x_{XPS} the Ga content) and σ the photoionization cross section of the core-level for the Al-Kα source given by [31]. As In4d and Ga3d core levels have very close kinetic energies (approximatively 1463 eV and 1465 eV, respectively, with the Al-Kα source), the ratio of their inelastic mean free path (IMFP) can be considered to be equal to 1 within the InGa lattice.

Then Equation 1 leads to the determination of indium content x_{XPS} by XPS :

$$x_{XPS} = \frac{R_{XPS}}{R_{XPS} + \frac{\sigma_{In4d}}{\sigma_{Ga3d}}} \#(2)$$

To achieve the decomposition of Ga3d and In4d core-levels using the CASA-XPS software [32], Shirley background and a SGL(10) Gaussian-Lorentzian mix function (with 10% Lorentzian content) are used for Ga3d line shape and Asymmetric Lorentzian LA(1.1,2.2,3) for $In_{(met)}$4d line shape. Spin orbit splitting is 0.45 eV and 0.89 eV for Ga3d and In4d, respectively, and the d5/2 and d3/2 doublet is constrained to have 3:2 peak area ratios. As XPS decompositions do not allow to distinguish gallium contribution coming from pure gallium environment and gallium in an indium environment, only one contribution is used for metallic Ga ($Ga_{(met)}$3d). Same assumption is considered for indium, using only one contribution ($In_{(met)}$4d), as shown in Fig. 2.

Note that binding energy scale is calibrated according to As-Ga $3d_{5/2}$ bond (E_b=41.1 eV) as realised in [33]. Decomposition of As3d core level is performed using SGL(10) function line shape, with a 0.69 eV spin orbit splitting and in respect with the 0.66 branch ratio (not shown here).

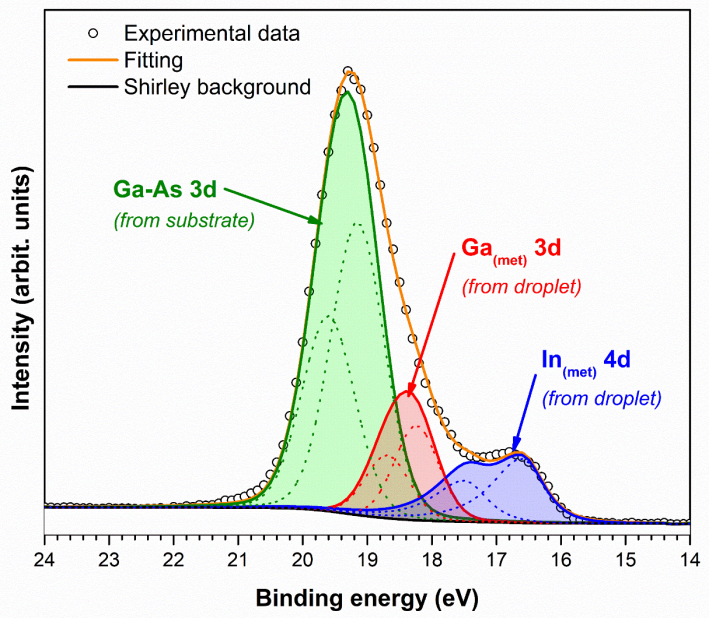

Fig. 2. XPS decomposition for InGa nanodroplets deposited on GaAs(111)A substrate. The dotted components show the 3/2 and 5/2 contributions of spin orbit splitting.

The uncertainty on the x_{XPS} value can be estimated by propagating the uncertainties of the intensity of Ga3d(met) and In4d(met) core level by considering a 10% variation of the RMS (root mean square). Also, we assume that there is no uncertainty on the values of the photoionization cross sections.

$$\frac{\Delta x_{XPS}}{x_{XPS}} = \frac{R_{XPS} \times \frac{\sigma_{In4d}}{\sigma_{Ga3d}}}{\left(R_{XPS} + \frac{\sigma_{In4d}}{\sigma_{Ga3d}}\right)^2} \times \sqrt{\left(\frac{\Delta I_{In4d(met)}}{I_{In4d(met)}}\right)^2 + \left(\frac{\Delta I_{Ga3d(met)}}{I_{Ga3d(met)}}\right)^2} \quad \#(3)$$

Note that the decomposition procedure leads to a higher uncertainty for $Ga_{(met)}3d$ intensity than for $In_{(met)}4d$ because of its intermediate location between Ga-As 3d and $In_{(met)}4d$ contributions.

2.3. Decomposition methodology of loss probabilities spectra from REELS

2.3.1. Bulk and surface plasmons

As XPS does not provide information of the precise chemical environment inside the metallic droplet, we propose to perform REELS because the study of the plasmons in REELS allows a material-sensitive study. Figure 3a shows REELS spectra, the region where losses from plasmon excitation occur; i.e. typically around 0-40 eV below the elastic peak. Plasmon results from the collective oscillation of the outer-shell electrons of a material. Inside the material, bulk plasmon (BP) energy is given by [34] :

$$\hbar\omega_p = \hbar\sqrt{\frac{n_v e^2}{\varepsilon_0 m_e}} \#(4)$$

Where e is the elementary charge, ε_0 the vacuum permittivity, m_e the mass of the electron and n_v the density of outer-shell electrons that can be estimated using the Equation 5 :

$$n_v(A_xB_y) = N_a \times \rho(A_xB_y) \times \frac{n_{th}}{M(A_xB_y)} \#(5)$$

There, A_xB_y is a material with x and y stoichiometry, N_a is Avogadro constant, ρ the density of the element, M the molar mass, n_{th} the theoretical number of outer-shell electrons: $n_{th} = x \times n_A + y \times n_B$ and n_i is the number of valence electrons of the element i.

Rupture of the continuum of the electronic cloud at the surface between the material and the vacuum is at the origin of the so-called surface plasmon (SP). Energy of SP for a planar interface with the vacuum, in the nearly-free electron approximation, can be estimated versus BP energy [35] :

$$\hbar\omega_s = \frac{\hbar\omega_p}{\sqrt{2}} \#(6)$$

2.3.2. From REELS raw experimental data to λK loss probabilities spectra

From REELS raw experimental data (Fig. 3a), loss probabilities curve (Fig. 3b) can be calculated using QUASES-XS-REELS software developed by S. Tougaard [36–39]. First step of the procedure is the correction for multiple scattered electrons, based on the universal inelastic scattering cross sections $K(E_0,E)$ as developed in references [37,40–42]. $K(E_0,E)dE$ represents the probability for an incoming E_0-energetic electron to loose energy in the range [E, E+dE]. It is well established that the general behaviour of this cross section can be described with universal formula valid for different classes of materials. Next step consists in the calculation of the product $\lambda \cdot K(E_0, E)$ where λ is the inelastic mean free path (IMFP). The $\lambda \cdot K(E_0, E)$ represents the inelastic scattering probability of electrons. This is the probability for electrons having a primary energy E_0 to lose an energy E in one inelastic interaction, normalised to the elastic peak. Note that calculation inaccuracies can occur for energy losses in the range of the replicas, that are multiple losses caused by the excitation of two or several plasmons [36,43,44] because first step is based on single-event loss.

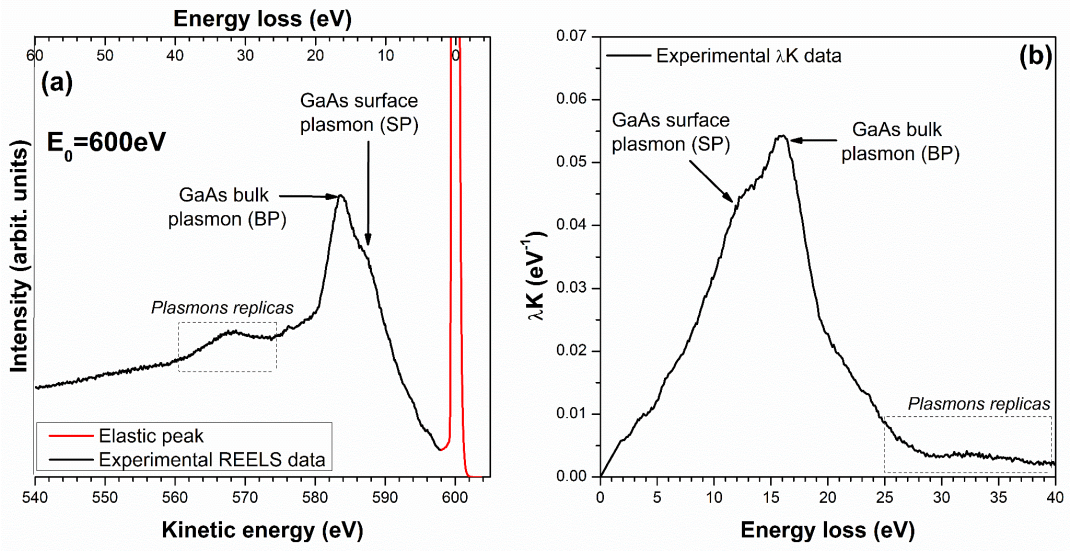

Fig. 3. From (a) REELS experimental data acquired for cleaned GaAs with primary energy E_0=600 eV to (b) λK loss probabilities curve calculated using QUASES-XS-REELS software.

2.3.3. REELS spectra of reference surfaces (GaAs, Ga and In)

2.3.3.1. GaAs(111)A

The functions, we use to achieve decomposition of the λK curve (Fig. 3b), are a Gaussian/Lorentzian mix with an arbitrary 10% Lorentzian content. To reduce the total degree of freedom of the decomposition, the same FWHM is kept between the bulk and surface plasmons. Also, all the other contributions have the same FWHM between them, but it can differ between single and multiple losses. Decompositions are then obtained by a weighted least-squares fitting using the CASA-XPS software [32]. Fig. 4 shows the loss probabilities curve decomposition for E_0=600 eV and 1500 eV acquired on a GaAs(111)A cleaned as previously described.

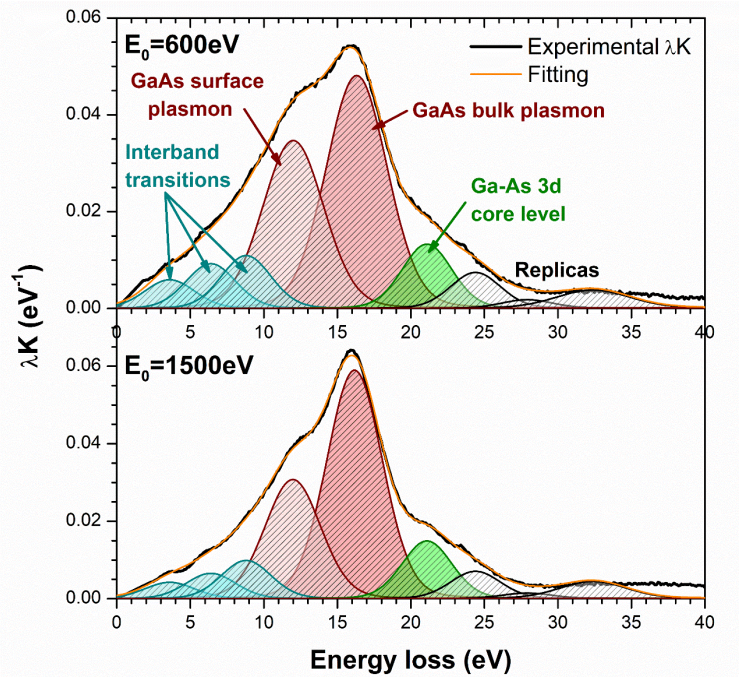

Fig. 4. Decomposition of GaAs loss probabilities curve for E_0=600 eV (top) and E_0=1500 eV (bottom).

The different inelastic contributions of GaAs(111)A are summarized in the Table 1. The observed GaAs BP energy (16.2 eV) is slightly higher than the theoretical value (15.6 eV), but remains close to values reported in the literature [45–50]. SP is also slightly higher than the values quoted in the literature [46,49]. Note that relation between BP and SP energies gives a 1.35 report close to the theoretical ratio of $\sqrt{2}$. Also, we notice that relative intensity between BP and SP depends on the primary energy. While E_0 increases, the SP intensity decreases compared to BP's, in good agreement with the probing depth. Among the three contributions that are needed to achieve a correct fitting for low energy losses (below 10 eV), two of them are used by N. Pauly *et al.* (at respectively 3.65 and 6.40 eV) to model GaAs energy loss functions [47]. Such contributions are attributed to interband transitions [48]. The contribution at 21.1eV is ascribed to the excitation of Ga-As 3d core-level as mentioned in [48], quite close to the 19.5 eV commonly found in XPS [33]. This slightly higher value in REELS can be explained by the XPS binding energy of core level being related to the Fermi level, that is not the case in REELS. Finally, we added three other contributions attributed to multiple losses replicas. However, we might be careful in this loss region because of the inaccuracies that occur during the Tougaard procedure as mentioned earlier. These contributions only allow the fitting adjustment.

Table 1

Energy, FWHM and physical interpretation of λK contributions for GaAs, Ga and In. Right column presents the contribution that are used for InGa droplets.

	GaAs(111)A (substrate)		**Gallium (from reference sample)**		**Indium (from reference sample)**		**In_xGa_{1-x} droplets from In and Ga references**	
Physical interpre-tation	**Posi-tion (eV)**	**FWHM (eV)**	**Position (eV)**	**FWHM (eV)**	**Position (eV)**	**FWHM (eV)**	**Posi-tion (eV)**	**FWHM (eV)**
Interband transition (IB)	3.6	4.0	3.7	4.0	3.5	4.0	3.6	4.0
	6.4		7.7		7.3		7.5	
	8.8							
Surface plasmon (**SP**)	11.9	Varies with E_0	10.1	Varies with E_0	8.5	Varies with E_0	Free	
Bulk plasmon (**BP**)	16.2		14.0		11.4			
d core-level excitation	21.1 (Ga3d)	4.0	19.8 (Ga3d)	3.2	18.2 (In4d)	3.2	19.0	3.2
Others (replicas)	Fitting adjustment							

2.3.3.2. *Pure indium and gallium*

Figure 5 shows the λK decomposition for (a) pure gallium and (b) pure indium at a primary electron energy E_0=1200 eV. The different inelastic contributions of Ga and In are summarized in the Table 1.

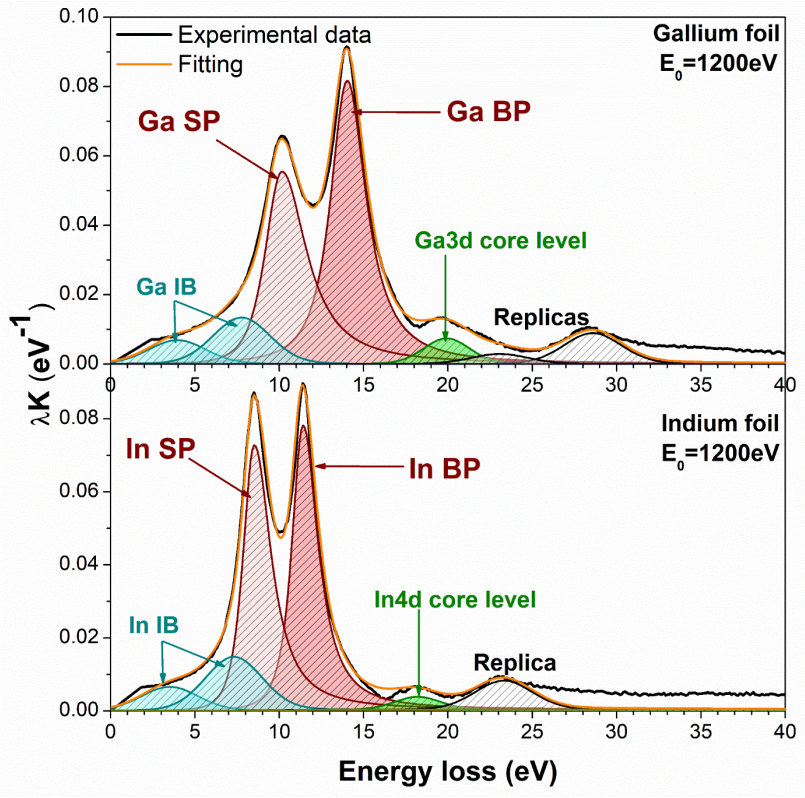

Fig. 5. λK decomposition acquired for a E0=1200 eV primary energy for (a) gallium and (b) indium.

The recorded gallium BP energy (14.0 eV) is close to the theoretical value of 14.4 eV. This value has already been quoted in the literature [45,51,52]. The recorded indium BP energy (11.4 eV) differs from the theoretical value of 12.6 eV. However, our value is close to other experimental values quoted in many references [29,45,51,53]. One can note that ratio between BP and SP energies are again close to $\sqrt{2}$ for both materials (1.39 for Ga and 1.34 for In). Note also that, for all the materials, BP and SP energies are independent of primary energy E_0. The use of asymmetric line shapes for metallic bulk and surface plasmons is required to accurately achieve the fit. This asymmetry for the higher loss energy has already been experimentally observed for aluminium [54–56] and silver [57]. Also, two contributions in the low loss energy range (3-8 eV) are attributed to interband transitions, as briefly quoted in the literature for indium [29]. Finally, as previously shown for Ga3d core-level in GaAs, primary electrons can excite d core-levels (Ga3d and In4d, respectively) close to values commonly found in XPS. Excitation of In4d in REELS has already been mentioned in [29,53]. Note that In4d value is smaller than metallic Ga3d value which is smaller than Ga3d value for GaAs, showing a physical consistency of our decomposition work.

2.3.3.3. Evolution of the plasmons FWHM with the primary electron energy E_0

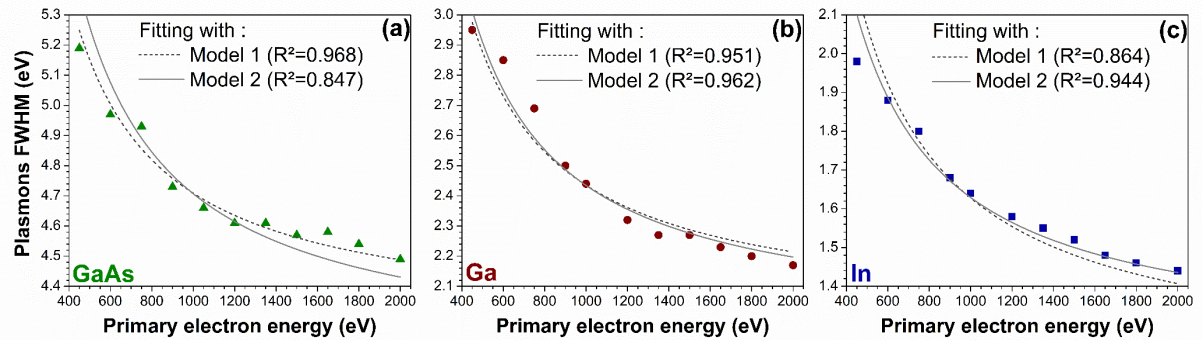

Fig. 6. Evolution of plasmons FWHM with the primary energy for (a) GaAs (b) Ga and (c) In.

According to our decompositions for GaAs, Ga and In, Fig. 6 shows the decrease of plasmons FWHM while the primary energy E_0 increases. Such phenomenon has been experimentally observed for indium [29] and aluminium [43,58] but never for Ga nor GaAs. Because semiconductors plasmons have higher FWHM than metals, it is more difficult to observe this evolution for GaAs without achieving the λK decomposition as we proceeded. This phenomenon is due to the increase of momentum transfer when the primary energy E_0 decreases [58–60]. The evolution can be fitted with the following equation:

$$\hbar\gamma(E_0) = \hbar\gamma_0 + \frac{C}{E_0} \quad \#(7)$$

Where $\hbar\gamma$ is the plasmon FWHM and $\hbar\gamma_0$ the limit of plasmons FWHM at high primary energies. As described in reference [55], two models arise for the value of C. In the first model, C is a material-independent constant whose value is $C=C_1=441.70$ eV². In the second model, $C = C_2 \times \hbar\omega_p$ where C_2 is also an material-independent variable ($C_2=33.91$ eV) and $\hbar\omega_p$ the material bulk plasmon energy. One can note that the first model gives a better fitting for GaAs, as opposed to indium, while both models are accurate for gallium.

2.3.4. Decomposition of loss probabilities for In_xGa_{1-x} droplets on GaAs(111)A

As the droplet height (4-5 nm [33]) is larger are higher than the IMFP of the electrons for the primary electron energy range we use (typically 600-1500 eV, leading to IMFP inferior to 3.5 nm), REELS signal can be separated into two sets of components gathering: the signal coming from the uncovered part of the substrate and the signal coming from the droplets.

2.3.4.1. Signal from the substrate

The inelastic contributions coming from substrate are gathered into an envelope, built with the three following rules:

(i) FWHM and positions of the substrate contributions (see Table 1) are found by the λK decomposition for the substrate before the droplet deposition.
(ii) The interband transitions and the surface plasmon intensities are normalised to the bulk plasmon intensity according to the λK decomposition for the substrate before the droplet deposition.
(iii) Plasmon replicas and Ga3d core-level are not included in the envelope because of the uncertainties in this loss region, as previously discussed.

Given our hypothesis about the height of the droplet superior to the IMFP of the primary electrons in the droplet, the interface plasmon created between the covered substrate and the droplet is neglected.

2.3.4.2. Signal coming from the In_xGa_{1-x} droplets

Based on the decompositions for pure Ga and In, we can define some of the inelastic contributions required for In_xGa_{1-x} alloy loss probabilities curve (see Table 1). The two interband transitions are defined at energies corresponding to the average value of In and Ga ones because they are close. For the same reason, In4d and Ga3d core level excitations are gathered in one contribution. As the replicas part of the spectra do not impact the bulk and surface plasmon decomposition, three free peaks are used to adjust the fit. By means of these parameters, the evolution of indium content x is related to the energies of In_xGa_{1-x} bulk (between 14.0 eV for Ga and 11.4 eV for In) and surface (between 10.1 eV and 8.5 eV) plasmons contributions using asymmetric shapes. The energy and FWHM of In_xGa_{1-x} plasmons are free parameters that will be adjusted during the fitting procedure. In a next part, we develop a semi-empirical formula to estimate indium percentage x from the energy of the In_xGa_{1-x} bulk plasmon. Such idea to use bulk plasmon energy to determine composition has already been developed by Williams and Edington to study Al and Mg alloys [61,62]. Note also that, using EELS in a TEM, Kong et al. [63] have shown a linear shift for $In_xGa_{1-x}N$ bulk plasmon energy according to indium percentage x.

2.3.4.3. Estimation of the coverage rate by REELS

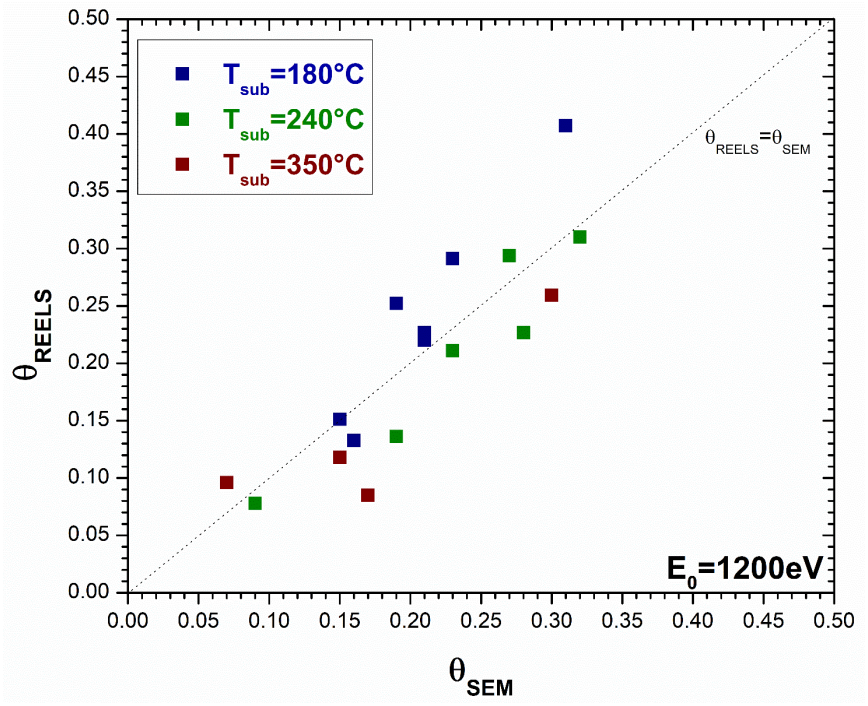

Fig. 7. Comparison of coverage rate values estimated by REELS and SEM.

Because the loss probabilities curves are normalised to the elastic peak and under the assumption previously developed that the electrons do not reach the wafer/droplet interface, the ratio between the intensities of the substrate BP after and before the droplet deposition can be written:

$$R_{REELS} = \frac{I_{substrate\ BP}(\text{after deposition})}{I_{substrate\ BP}(\text{before deposition})} = 1 - \theta \ \#(8)$$

Leading to the estimation by REELS of the coverage rate θ:

$$\theta_{REELS} = 1 - R_{REELS} \ \#(9)$$

Figure 7 shows the comparison of the coverage rate θ estimated by both REELS and SEM for each sample (with different R_f and T_{sub}). The right overall agreement between these two values acts as a validation of our decomposition methodology separating REELS signal from the droplet and from the substrate.

2.3.5. Semi-empirical model for the determination from REELS of indium/gallium content in the droplet

The theoretical values of BP energy for a given material can be calculated from Equation 4. However, we showed some inaccuracies for theoretical values compared to experimental values, in particular for indium. To fix this issue, the notion of the efficient density valence electron n_v^{eff} corresponding to the density of electrons that actually contribute to the plasma

oscillation is introduced. This density can be empirically estimated from experimental bulk plasmon energies E_{BP}^{exp}:

$$n_v^{eff} = \frac{\epsilon_0 m_e}{e^2} \times \left(\frac{\hbar\omega_p^{exp}}{\hbar} \right)^2 \quad \#(10)$$

giving the values of $n_v^{eff} = 1.40 \times 10^{29}\ cm^{-3}$ for gallium and $n_v^{eff} = 0.94 \times 10^{29}\ cm^{-3}$ for indium (instead of $n_v = 1.53 \times 10^{29}\ cm^{-3}$ and $n_v = 1.15 \times 10^{29}\ cm^{-3}$, corresponding to a relative difference of 8% and 18%, respectively). Now, by considering the hypothesis of a linear evolution of the valence electron density (here, the effective one), we can estimate the bulk plasmon energy of In_xGa_{1-x} by:

$$\hbar\omega_p(In_xGa_{1-x}) = \sqrt{\frac{e^2}{\epsilon_0 m_e}} \times \sqrt{x \times n_v^{eff}(In) + (1-x) \times n_v^{eff}(Ga)} \quad \#(11)$$

That can be rewritten in a strictly equivalent way as:

$$\hbar\omega_p(In_xGa_{1-x}) = \hbar\omega_p(Ga) \times \sqrt{\frac{x \times n_v^{eff}(In) + (1-x) \times n_v^{eff}(Ga)}{n_v^{eff}(Ga)}} \quad \#(12)$$

One can note that the Equation 12 gives a trend very close to the linear evolution (R^2>0.99) shown in [63] . Finally, from this equation, the REELS indium content can be determined:

$$x_{REELS} = \frac{n_v^{eff}(Ga) \times \left[1 - \left(\frac{\hbar\omega_p(In_xGa_{1-x})}{\hbar\omega_p(Ga)}\right)^2\right]}{n_v^{eff}(Ga) - n_v^{eff}(In)} \quad \#(13)$$

In_xGa_{1-x} bulk plasmon energy is obtained by considering the mean value for four different primary energies (600, 900, 1200 and 1500 eV). Uncertainties on the x_{REELS} values are calculated by propagating a ±0.10 eV uncertainty for each plasmon energy (Ga and In from reference decomposition and In_xGa_{1-x} from droplets decomposition):

$$\Delta x_{REELS} = \sqrt{(\Delta x_{REELS}|_{Ga})^2 + (\Delta x_{REELS}|_{In})^2 + (\Delta x_{REELS}|_{InGa})^2} \quad \#(14)$$

Where :

$$\Delta x_{REELS}|_i = \left|\frac{\partial x_{REELS}}{\partial \hbar\omega_p(i)}\right| \times \Delta\hbar\omega_p(i) \ \ (i = Ga, In \text{ or } InGa) \#(15)$$

3. Results & discussion

Figure 8 shows XPS and REELS spectra decompositions for four samples of In_xGa_{1-x} droplets deposited on GaAs(111)A at a substrate temperature of $T_{substrate}$=180°C with different indium content, monitored by different R_f. Using the methodology previously developed, the rate x is calculated using the XPS and the REELS spectra.

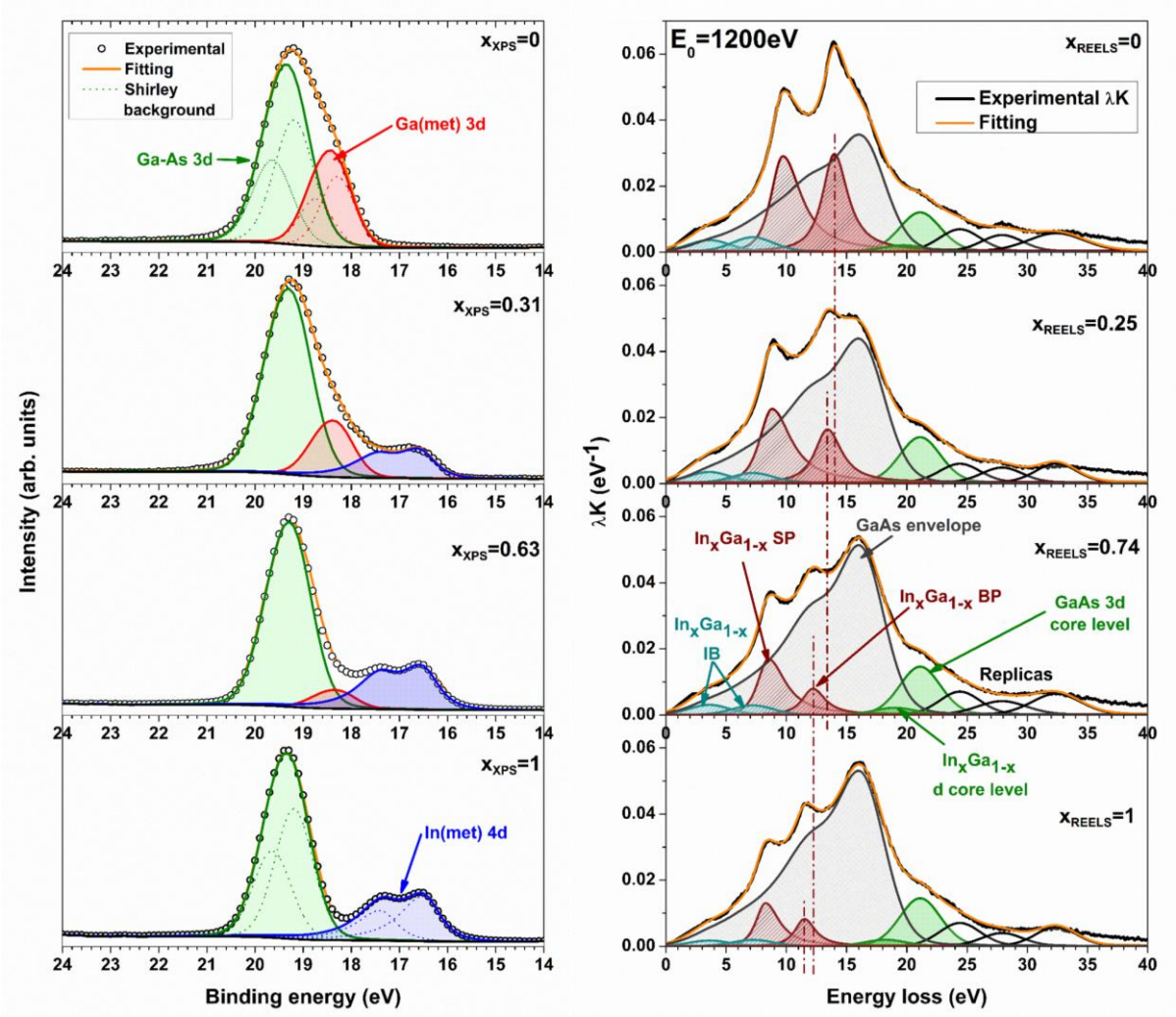

Fig. 8. Decomposition of Ga3d-In4d XPS spectra (left panel) and loss probabilities from REELS (right panel) for different compositions of In_xGa_{1-x} droplets self-assembled on GaAs(111)A substrate ($T_{substrate}$=180°C). Mixed lines on the REELS decompositions illustrate the shift of In_xGa_{1-x} bulk plasmon energy for the different compositions. Ga3d3/2 and 3d5/2 (In4d3/2 and 4d5/2) components are shown in dotted lines in XPS decompositions for Ga droplets (x_{XPS}=0) (for In droplets (x_{XPS}=1)).

The values of BP energy for pure Ga (In) droplets are similar to the values for Ga (In) foil previously shown. That shows no size effect on the BP energy for droplets with diameter superior to 15 nm [33]. Such size effect has already been experienced on CdS quantum dots [64] and Si clusters [65] for particles but with a very small diameter (< 5 nm).

Note that for pure In and Ga droplets, SP energies are slightly lower by about 0.2 eV than for foils. A recent study of TEM loss spectra of individual lens-shaped gallium nanodroplets [52]

ascribes a 7.4 eV transition to the Ga SP. However, our work shows the Ga SP is rather located around 10 eV, even for nanodroplets, and we ascribe the contribution at 7.7 eV to interband transition. In [52], the authors also point to an interesting contribution at 3.3 eV (also shown in our work), attributed to dipole-localized surface plasmon, whose energy is correlated to the nanodroplet size.

Red mixed lines in the Fig. 8 shows the energy shift of In_xGa_{1-x} BP from 14.0 eV (pure Ga droplets) to 11.5 eV (pure In droplets). Note that, whatever the composition, the FWHM of In_xGa_{1-x} plasmons increases while primary electron energy E_0 decreases, as discussed previously. REELS decompositions are therefore easier to achieve for primary energies beyond 1000 eV and lead to greater uncertainties for lower primary energies because of the increase of plasmons FWHM.

From REELS and XPS decompositions and using equations 2 and 13, we can compare for each sample the values of x_{REELS} and x_{XPS}, as shown in Fig. 9.

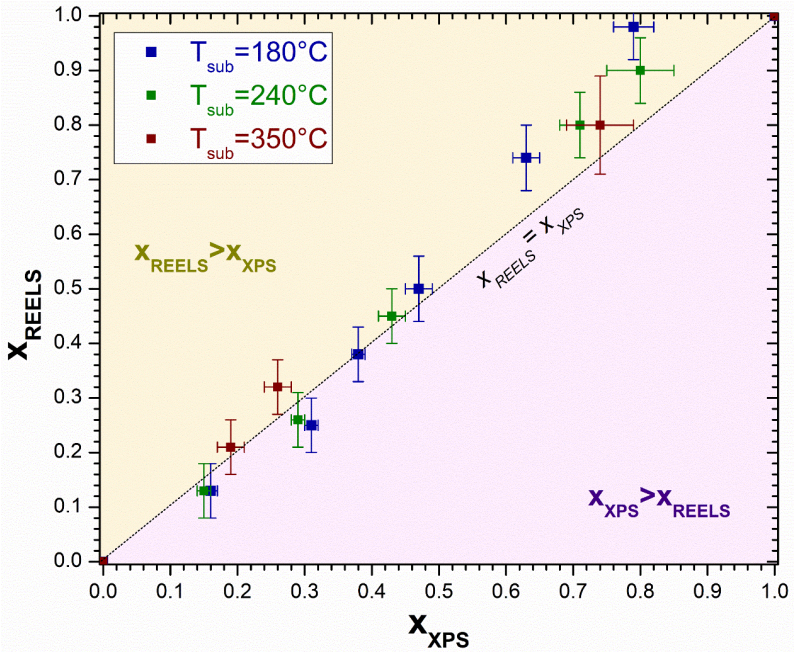

Fig. 9. Comparison of the values x obtained with XPS and REELS.

For low indium contents (x<0.50), by considering the uncertainties, one can consider XPS and REELS values for indium gallium composition as broadly close. That leads to the conclusion of a good In/Ga mixing to form homogeneous InGa droplets while x<0.50.

For high indium contents (x>0.70), uncertainty on XPS values is higher than for low indium content because of a smaller $Ga_{(met)}$3d core level intensity. Global trend however shows a REELS value higher than XPS value (yellow area). However, the deviation between the REELS and XPS results for high indium contents cannot be due only to the uncertainties. Even more striking, the top blue point shows the deposition of an x_{XPS}=0.79 indium content while REELS shows quasi pure indium droplets (x_{REELS}≈1). For high indium contents, these results suggest that the mixing of gallium and indium is not complete, leading to two assumptions.

Firstly, the lack of mixing between In and Ga might be caused by phase separation inside the droplet for high indium contents according to the phase diagram for the In_xGa_{1-x} alloy [66].

According to this phase diagram, high indium content alloy could have a richer indium phase, in good agreement with the results obtained by the combination of XPS and REELS. In order to verify this possibility, we performed the simultaneous deposition of indium and gallium with an R_f=0.9 indium relative flux for a 180°C substrate temperature. XPS gives a 0.71 indium content while REELS gives around 0.86, showing again the discrepancies between these two values for high indium contents. Then, we proceeded to a heating of the sample from room temperature to 270°C while performing REELS for several temperatures. However, the variation of In_xGa_{1-x} BP energy with the temperature is not significant enough to consider that heating or cooling could impact the droplet composition. Moreover, we have also performed REELS for higher primary energies (2000 and 3000 eV), leading to a deeper depth analysis. Rich indium droplets BP energy is the same for low primary energies than for high primary energies, showing that the phase separation hypothesis does not seem to explain the differences observed between REELS and XPS values of composition.

A second possibility is to consider that some of gallium atoms are not integrated into the InGa droplets, forming two droplets families which are respectively rich-indium InGa droplets and pure Ga droplets. However, we cannot distinguish neither BP nor SP for pure gallium in the loss probabilities decomposition whatever the primary energy, potentially explainable by the low amount of Ga remaining out of the droplet. We could put forward the hypothesis that such phenomena may be caused by the low Ga flux preventing gallium from being fully incorporated into InGa droplets. However, nor can XPS provide any other information about it because modelling the intensities for each of the two situations (lack of incorporation or phase separation) involves too many unknown input parameters. Thus the XPS model used (considering a homogeneous droplet composition) in the Fig. 9 becomes inappropriate to the droplet organisation for high indium contents.

We show here that the complementary use of XPS and REELS offers a unique opportunity to investigate the indium and gallium mixing to grow self-assembled InGa droplets. Table 2 summarizes benefits and drawbacks for each spectroscopy, showing their strong complementary. Even if the cause of inhomogeneity for high-indium content still remains unsolved, the ability to grow homogeneous 10% to 50% indium content In_xGa_{1-x} nanodroplets on GaAs(111)A offers promising results for the growth of $In_xGa_{1-x}N$ quantum dots by the DE.

Table 2

Benefits and drawbacks of XPS and REELS showing the strong interest for a complementary use.

	XPS	**REELS**
Employed method to determine x_{In}	Intensity ratio $R_{XPS} = \frac{I_{In4d(met)}}{I_{Ga3d(met)}}$	In_xGa_{1-x} bulk plasmon energy determined from λK decomposition
Surface sensitivity	Typically < 10 nm (Al-Kα anode)	< 4 nm Tuneable by varying primary energy
Spectra acquisition time	Around 1h (survey + core-levels)	Few minutes for each primary energy
Benefits	Widely used electronic spectroscopy Quantification easily achievable from XPS decomposition and intensity ratio R_{XPS}	Easy to set-up As plasmons are a collective phenomenon, REELS is material-sensitive, leading to information about the droplet composition, alloy and eventual segregation. The envelope methodology can be extended to a large range of systems.
Drawbacks	XPS does not provide information about alloy and eventual segregation	λK decompositions are complex and requires the use of the envelope method and standard samples.
Uncertainties about indium content x	$\Delta x_{XPS} = 0.01 - 0.03$ from intensity ratio uncertainties Uncertainty varies with the composition.	$\Delta x_{REELS} \sim 0.05$ from bulk plasmon energy uncertainties (±0.10 eV) Uncertainty does not vary with the composition.

4. Conclusion

The development of a new spectroscopic tool based on the complementary use of XPS and REELS allows to *in situ* characterize indium/gallium composition in In_xGa_{1-x} droplets self-assembled on GaAs(111)A. An important part of this work relies on the decomposition methodology for REELS loss probabilities curve based on reference samples and the envelope method allowing to separate inelastic contributions from the substrate and the droplets. Then, the material-sensitive REELS provides information about the indium/gallium content in the droplet using the In_xGa_{1-x} BP energy. On the other hand, XPS, based on intensity ratio between In4d and Ga3d core-levels, can also provide the composition of the droplet but requires the assumption of homogeneous droplets. The complementary use of these two electronic spectroscopies is then required to study the In/Ga mixing to grow In_xGa_{1-x} self-assembled droplets on GaAs(111)A. This work also highlights for the first time to our knowledge the ability to grow such In_xGa_{1-x} droplets with an indium content varying in the whole range from 0 to 100%. Even if integration of gallium in indium-rich condition of deposit is not total, we show a very good In/Ga mixing for indium content below 70%. These are very

promising results for the growth of $In_xGa_{1-x}N$ quantum dots on GaAs(111)A by droplet epitaxy, for the whole range of composition.

Aknowlegdments

The authors gratefully acknowledge financial support from the project SASS AV0027152 from FEDER-FSE-2014-2020 and the project 16-IDEX-0001 CAP 20-25.

References

[1] S. Deshpande, T. Frost, A. Hazari, P. Bhattacharya, Electrically pumped single-photon emission at room temperature from a single InGaN/GaN quantum dot, Appl Phys Lett 105 (2014) 141109. https://doi.org/10.1063/1.4897640.

[2] Y. Mei, G.E. Weng, B.P. Zhang, J.P. Liu, W. Hofmann, L.Y. Ying, J.Y. Zhang, Z.C. Li, H. Yang, H.C. Kuo, Quantum dot vertical-cavity surface-emitting lasers covering the “green gap,” Light Sci Appl 6 (2017) 1. https://doi.org/10.1038/lsa.2016.199.

[3] H. Li, P. Li, J. Kang, J. Ding, J. Ma, Y. Zhang, X. Yi, G. Wang, Broadband full-color monolithic InGaN light-emitting diodes by self-assembled InGaN quantum dots, Sci Rep 6 (2016) 1. https://doi.org/10.1038/srep35217.

[4] N. Grandjean, M. Ilegems, Visible InGaN/GaN quantum-dot materials and devices, in: Proceedings of the IEEE, 2007: p. 1853. https://doi.org/10.1109/JPROC.2007.900970.

[5] J. Kasemchainan, C. Kuss, D.E.J. Armstrong, D. Cai, R.J. Wallace, F.H. Richter, H.J. Thijssen, P.G. Bruce, Polarisation-controlled single photon emission at high temperatures from InGaN quantum dots, Nanoscale 9 (2018) 9421. https://doi.org/10.1039/c7nr03391e.

[6] J.S. Kim, M.S. Jeong, C.C. Byeon, D.K. Ko, J. Lee, J.S. Kim, I.S. Kim, N. Koguchi, GaAs quantum dots with a high density on a GaAs (111) A substrate, Appl Phys Lett 88 (2006) 2004. https://doi.org/10.1063/1.2213012.

[7] A. Tuktamyshev, A. Fedorov, S. Bietti, S. Tsukamoto, S. Sanguinetti, Temperature Activated Dimensionality Crossover in the Nucleation of Quantum Dots by Droplet Epitaxy on GaAs(111)A Vicinal Substrates, Sci Rep 9 (2019) 1. https://doi.org/10.1038/s41598-019-51161-5.

[8] C.L. Wu, L.J. Chou, S. Gwo, Size- and shape-controlled GaN nanocrystals grown on Si(111) substrate by reactive epitaxy, Appl Phys Lett 85 (2004) 2071. https://doi.org/10.1063/1.1787947.

[9] T. Kondo, K. Saitoh, Y. Yamamoto, T. Maruyama, S. Naritsuka, Fabrication of GaN dot structures on Si substrates by droplet epitaxy, Physica Status Solidi (A) Applications and Materials Science 203 (2006) 1700. https://doi.org/10.1002/pssa.200565212.

[10] H. Lu, C. Reese, S. Jeon, A. Sundar, Y. Fan, E. Rizzi, Y. Zhuo, L. Qi, R.S. Goldman, Mechanisms of GaN quantum dot formation during nitridation of Ga droplets, Appl Phys Lett 116 (2020) 062107. https://doi.org/10.1063/1.5133965.

[11] G. Tsamo, A.G. Nastovjak, N.L. Shwartz, P.E. Hoggan, C. Robert-Goumet, A. Pimpinelli, M. Petit, A. Ranguis, E. Gardes, M. Sall, L. Bideux, G. Monier, Growth Mechanisms of GaN/GaAs Nanostructures by Droplet Epitaxy Explained by Complementary Experiments and Simulations, The Journal of Physical Chemistry C 128 (2024). https://doi.org/10.1021/acs.jpcc.3c07945.

[12] M. Refaei, A. Kuchuk, R. Allaparthi, M. Sarollahia, M.H.U. Maruf, M.E. Ware, Controlling the size and density of InN quantum dots formed on sapphire substrate by droplet epitaxy, Journal of Vacuum Science & Technology A 41 (2023) 042711. https://doi.org/10.1116/6.0002679.

[13] M. Kumar, B. Roul, T.N. Bhat, M.K. Rajpalke, N. Sinha, A.T. Kalghatgi, S.B. Krupanidhi, Droplet epitaxy of InN quantum dots on Si(111) by RF plasma-assisted molecular beam epitaxy, Adv Sci Lett 3 (2010) 379. https://doi.org/10.1166/asl.2010.1163.

[14] P. Aseev, Gačević, J.M. Mánuel, J.J. Jiménez, R. García, F.M. Morales, E. Calleja, Formation mechanisms of single-crystalline InN quantum dots fabricated via droplet epitaxy, J Cryst Growth 493 (2018) 65. https://doi.org/10.1016/j.jcrysgro.2018.04.027.

[15] N. Nurzal, T. Yu, H. Iwan, I.S. Yu, Droplet epitaxy of InGaN quantum dots on Si (111) by plasma-assisted molecular beam epitaxy, Discover Nano 18 (2023) 60. https://doi.org/10.1186/s11671-023-03844-2.

[16] M.E. Vickers, M.J. Kappers, T.M. Smeeton, E.J. Thrush, J.S. Barnard, C.J. Humphreys, Determination of the indium content and layer thicknesses in InGaN/GaN quantum wells by x-ray scattering, J Appl Phys 94 (2003) 1565. https://doi.org/10.1063/1.1587251.

[17] Y. Zhao, J.C. Zhang, J.S. Xue, X.W. Zhou, S.R. Xu, Y. Hao, Influence of compressive strain on the incorporation of indium in InGaN and InAlN ternary alloys, Chinese Physics B 24 (2015) 017302. https://doi.org/10.1088/1674-1056/24/1/017302.

[18] F.K. Yam, Z. Hassan, InGaN: An overview of the growth kinetics, physical properties and emission mechanisms, Superlattices Microstruct 43 (2008) 1. https://doi.org/10.1016/j.spmi.2007.05.001.

[19] I.G. Vasileiadis, L. Lymperakis, A. Adikimenakis, A. Gkotinakos, V. Devulapalli, C.H. Liebscher, M. Androulidaki, R. Hübner, T. Karakostas, A. Georgakilas, P. Komninou, E. Dimakis, G.P. Dimitrakopulos, Substitutional synthesis of sub-nanometer InGaN/GaN quantum wells with high indium content, Sci Rep 11 (2021) 1. https://doi.org/10.1038/s41598-021-99989-0.

[20] M. Schuster, P.O. Gervais, B. Jobst, W. Hösler, R. Averbeck, H. Riechert, A. Iberl, R. Stömmer, Determination of the chemical composition of distorted InGaN/GaN heterostructures from X-ray diffraction data, J Phys D Appl Phys 32 (1999) A56. https://doi.org/10.1088/0022-3727/32/10A/312.

[21] S.M. Hamad, D.P. Norman, Q.Y. Chen, F. Keles, H.W. Seo, Competitive In and Ga incorporations for InxGa1-xN (0.29<x<0.36) nanorods grown at a moderate temperature, AIP Adv 3 (2013) 072128. https://doi.org/10.1063/1.4816805.

[22] S. Berrah, A. Boukortt, H. Abid, Optical properties of the cubic alloy (In,Ga)N, Physica E 41 (2009) 701. https://doi.org/10.1016/j.physe.2008.11.009.

[23] L. Vegard, Die Konstitution der Mischkristalle und die Raumfüllung der Atome, Z. Physik 5 (1921) 17. https://doi.org/10.1007/BF01349680.

[24] T. Walther, Measuring Non-Destructively the Total Indium Content and Its Lateral Distribution in Very Thin Single Layers or Quantum Dots Deposited onto Gallium Arsenide Substrates Using Energy-Dispersive X-ray Spectroscopy in a Scanning Electron Microscope, Nanomaterials 12 (2022). https://doi.org/10.3390/nano12132220.

[25] E. Roche, Y. André, G. Avit, C. Bougerol, D. Castelluci, F. Réveret, E. Gil, F. Médard, J. Leymarie, T. Jean, V.G. Dubrovskii, A. Trassoudaine, Circumventing the miscibility gap

in InGaN nanowires emitting from blue to red, Nanotechnology 29 (2018) 465602. https://doi.org/10.1088/1361-6528/aaddc1.

[26] B. Qi, S. Shayestehaminzadeh, S. Ólafsson, M. Göthelid, H.P. Gislason, Formation and nitridation of InGa composite droplets on Si(1 1 1): In-situ study by high resolution X-ray photoelectron spectroscopy, Appl Surf Sci 303 (2014) 297–305. https://doi.org/10.1016/j.apsusc.2014.02.170.

[27] L. Medvecký, J. Briančin, Possibilities of simultaneous determination of indium and gallium in binary InGa alloys by anodic stripping voltammetry in acetate buffer, Chemical Papers 58 (2004) 93.

[28] O.E. Tereshchenko, V.L. Alperovich, A.S. Terekhov, Composition and structure of chemically prepared GaAs(1 1 1)A and (1 1 1)B surfaces, Surf Sci 600 (2006) 577. https://doi.org/10.1016/j.susc.2005.11.007.

[29] N. Pauly, A. Dubus, G. Monier, C. Robert-Goumet, M.A. Mahjoub, L. Bideux, B. Gruzza, Energy dependence of the energy loss function parametrization of indium in the Drude-Lindhard model, Surface and Interface Analysis 46 (2014) 283. https://doi.org/10.1002/sia.5411.

[30] C.S. Fadley, Basic Concepts of X-ray Photoelectron Spectroscopy, in: C.R. Brundle, A.D. Baker (Eds.), Electron Spectroscopy: Theory, Techniques and Applications, Academic P, 1981: pp. 1–156.

[31] J.H. Scofield, Hartree-Slater subshell photoionization cross-sections at 1254 and 1487 eV, J Electron Spectros Relat Phenomena 8 (1976) 129. https://doi.org/10.1016/0368-2048(76)80015-1.

[32] N. Fairley, V. Fernandez, M. Richard-Plouet, C. Guillot-Deudon, J. Walton, E. Smith, D. Flahaut, M. Greiner, M. Biesinger, S. Tougaard, D. Morgan, J. Baltrusaitis, Systematic and collaborative approach to problem solving using X-ray photoelectron spectroscopy, Applied Surface Science Advances 5 (2021) 100112. https://doi.org/10.1016/j.apsadv.2021.100112.

[33] G. Tsamo, G. Monier, P. Hoggan, C. Robert-goumet, M. Petit, A. Ranguis, L. Bideux, XPS modeling of GaN/GaAs nanostructure grown by the droplet epitaxy technique, J Electron Spectros Relat Phenomena 261 (2022) 147257. https://doi.org/10.1016/j.elspec.2022.147257.

[34] D. Bohm, D. Pines, A collective description of electron interactions: III. Coulomb interactions in a degenerate electron gas, Physical Review 92 (1953) 609. https://doi.org/10.1103/PhysRev.92.609.

[35] R.H. Ritchie, Plasma Losses by Fast Electrons in Thin Films, Physical Review 106 (1957) 874. https://doi.org/https://doi.org/10.1103/PhysRev.106.874.

[36] S. Tougaard, I. Chorkendorff, Differential inelastic electron scattering cross sections from experimental reflections electron-energy-loss spectra : Application to background removal in electron spectroscopy, Phys Rev B 35 (1987) 6570. https://doi.org/10.1103/PhysRevB.35.6570.

[37] S. Tougaard, Quantitative analysis of the inelastic background in surface electron spectroscopy, Surface and Interface Analysis 11 (1988) 453. https://doi.org/10.1002/sia.740110902.

[38] S. Tougaard, J. Kraaer, Inelastic-electron-scattering cross sections for Si, Cu, Ag, Au, Ti, Fe and Pd, Phys Rev B 43 (1991) 1651. https://doi.org/10.1103/PhysRevB.43.1651.

[39] S. Tougaard, Universality classes of inelastic electron scattering cross-sections, Surface and Interface Analysis 25 (1997) 137. https://doi.org/10.1002/(SICI)1096-9918(199703)25:3<137::AID-SIA230>3.0.CO;2-L.

[40] C. Jansson, H.S. Hansen, F. Yubero, S. Tougaard, Accuracy of the Tougaard method for quantitative surface analysis. Comparison of the Universal and REELS inelastic cross sections, J Electron Spectros Relat Phenomena 60 (1992) 301. https://doi.org/10.1016/0368-2048(92)80025-4.

[41] I. Chorkendorff, S. Tougaard, Background subtraction in electron spectroscopy by use of reflection electron energy loss spectra, Appl Surf Sci 29 (1987) 101. https://doi.org/10.1016/0169-4332(87)90018-3.

[42] M.P. Seah, I.S. Gilmore, S.J. Spencer, Background subtraction II. General behaviour of REELS and the Tougaard universal cross section in the removal of backgrounds in AES and XPS, Surf Sci 461 (2000) 1. https://doi.org/10.1016/S0039-6028(00)00373-3.

[43] T.S. Yubero, Model for quantitative analysis of reflection-eletron-energy-loss spectra, Phys Rev B 46 (1992) 2486. https://doi.org/10.1103/PhysRevB.46.2486.

[44] W.S.M. Werner, Differential surface and volume excitation probability of medium-energy electrons in solids, Phys Rev B 74 (2006) 075421. https://doi.org/10.1103/PhysRevB.74.075421.

[45] H. Raether, Excitation of Plasmons and Interband Transitions by Electrons, in: Springer Tracts in Modern Physics, Springer Berlin, Heidelberg, 1980. https://doi.org/https://doi.org/10.1007/BFb0045951.

[46] L. Bideux, D. Baca, B. Gruzza, V. Matolin, C. Robert-Goumet, Surface modification of GaAs during argon ionic cleaning and nitridation: EELS, EPES and XPS studies, Surf Sci 566–568 (2004) 1158. https://doi.org/10.1016/j.susc.2004.06.076.

[47] N. Pauly, S. Tougaard, Surface excitation parameter for 12 semiconductors and determination of a general predictive formula, Surface and Interface Analysis 41 (2009) 735. https://doi.org/10.1002/sia.3081.

[48] H. Jin, H. Shinotsuka, H. Yoshikawa, H. Iwai, M. Arai, S. Tanuma, S. Tougaard, Evaluation of robustness to surface conditions of the target factor analysis method for determining the dielectric function from reflection electron energy loss spectra: Application to GaAs, Surface and Interface Analysis 45 (2013) 985. https://doi.org/10.1002/sia.5196.

[49] V.M. Mikoushkin, A.P. Solonitsyna, E.A. Makarevskaya, Elemental arsenic in the natural oxide on the MBE GaAs surface, Appl Surf Sci 504 (2020) 144601. https://doi.org/10.1016/j.apsusc.2019.144601.

[50] N. Pauly, F. Yubero, S. Tougaard, ELF dielectric functions for various materials. (1.0) [Dataset], Zenodo (2022). https://doi.org/10.5281/zenodo.6024064.

[51] C.J. Powell, Characteristic Energy Losses of 8-keV Electrons in Liquid Al, Bi, In, Ga, Hg and Au, Physical Review 175 (1968) 972. https://doi.org/10.1103/PhysRev.175.972.

[52] M. Horák, V. Čalkovský, J. Mach, V. Křápek, T. Šikola, Plasmonic Properties of Individual Gallium Nanoparticles, Journal of Physical Chemistry Letters 14 (2023) 2012. https://doi.org/10.1021/acs.jpclett.3c00094.

[53] M. Bouslama, M. Ghamnia, B. Gruzza, F. Miloua, C. Jardin, AES and EELS analysis of the interaction between phosphorus and metallic indium, J Electron Spectros Relat Phenomena 68 (1994) 377. https://doi.org/10.1016/0368-2048(94)02137-6.

[54] P.C. Gibbons, S.E. Schnatterly, J.J. Ritsko, J.R. Fields, Line shape of the plasma resonance in simple metals, Phys Rev B 13 (1976) 2451. https://doi.org/10.1103/PhysRevB.13.2451.

[55] A. Sulyok, K. Tőkési, Surface and Bulk Plasmon Excitation on Aluminum Surface at Small to High Grazing Angles, Atoms 10 (2022) 104. https://doi.org/10.3390/atoms10040104.

[56] M. Dapor, L. Calliari, M. Filippi, REEL spectra from aluminium: Experiment and Monte Carlo simulation using two different dielectric functions, Surface and Interface Analysis 40 (2008) 683. https://doi.org/10.1002/sia.2711.

[57] M. Rocca, Low-energy EELS investigation of surface electronic excitations on metals, Surf Sci Rep 22 (1995) 1. https://doi.org/10.1016/0167-5729(95)00004-6.

[58] L. Calliari, M. Dapor, M. Filippi, Joint experimental and computational study of aluminum electron energy loss spectra, Surf Sci 601 (2007) 2270. https://doi.org/10.1016/j.susc.2007.03.029.

[59] Y. Ohno, Kramers-Kronig analysis of reflection electron-energy-loss spectra measured with a cylindrical mirror analyzer, Phys Rev B 39 (1989) 8209. https://doi.org/10.1103/PhysRevB.39.8209.

[60] M. Hasegawa, M. Watabe, Theory of plasmon damping in metal, J. Phys. Soc. Japan 27 (1969) 1393. https://doi.org/10.1143/JPSJ.27.1393.

[61] G. Hibbert, J.W. Edington, D.B. Williams, P. Doig, The variation of plasma energy loss with composition in dilute aluminium-magnesium solid solutions, Philosophical Magazine 26 (1972) 1491. https://doi.org/10.1080/14786437208220360.

[62] D.B. Williams, J.W. Edington, High resolution microanalysis in materials science using electron energy loss measurements, J Microsc 108 (1976) 113. https://doi.org/10.1111/j.1365-2818.1976.tb01086.x.

[63] X. Kong, S. Albert, A. Bengoechea-Encabo, M.A. Sanchez-Garcia, E. Calleja, A. Trampert, Plasmon excitation in electron energy-loss spectroscopy for determination of indium concentration in (In,Ga)N/GaN nanowires, Nanotechnology 23 (2012) 485701. https://doi.org/10.1088/0957-4484/23/48/485701.

[64] P.N.H. Nakashima, T. Tsuzuki, A.W.S. Johnson, Particle size dependence of the volume plasmon energy in cadmium sulphide quantum dots by electron energy loss spectroscopy, J Appl Phys 85 (1999) 1556. https://doi.org/10.1063/1.369337.

[65] M. Mitome, Y. Yamazaki, H. Takagi, T. Nakagiri, Size dependence of plasmon energy in Si clusters, J Appl Phys 72 (1992) 812. https://doi.org/10.1063/1.351820.

[66] B.C. Rugg, T.G. Chart, A critical assessment of thermodynamic and phase diagram data for the gallium-indium system, Calphad 14 (1990) 115. https://doi.org/10.1016/0364-5916(90)90013-P.